CHEMISTRY
A EUROPEAN JOURNAL

DOI: 10.1002/chem.201001806

The Dynamic Chemistry of Molecular Borromean Rings and Solomon Knots

Cari D. Meyer,[a] Ross S. Forgan,[b] Kelly S. Chichak,[a] Andrea J. Peters,[a] Nicholas Tangchaivang,[a] Gareth W. V. Cave,[c] Saeed I. Khan,[a] Stuart J. Cantrill,[a] and J. Fraser Stoddart*[a, b]

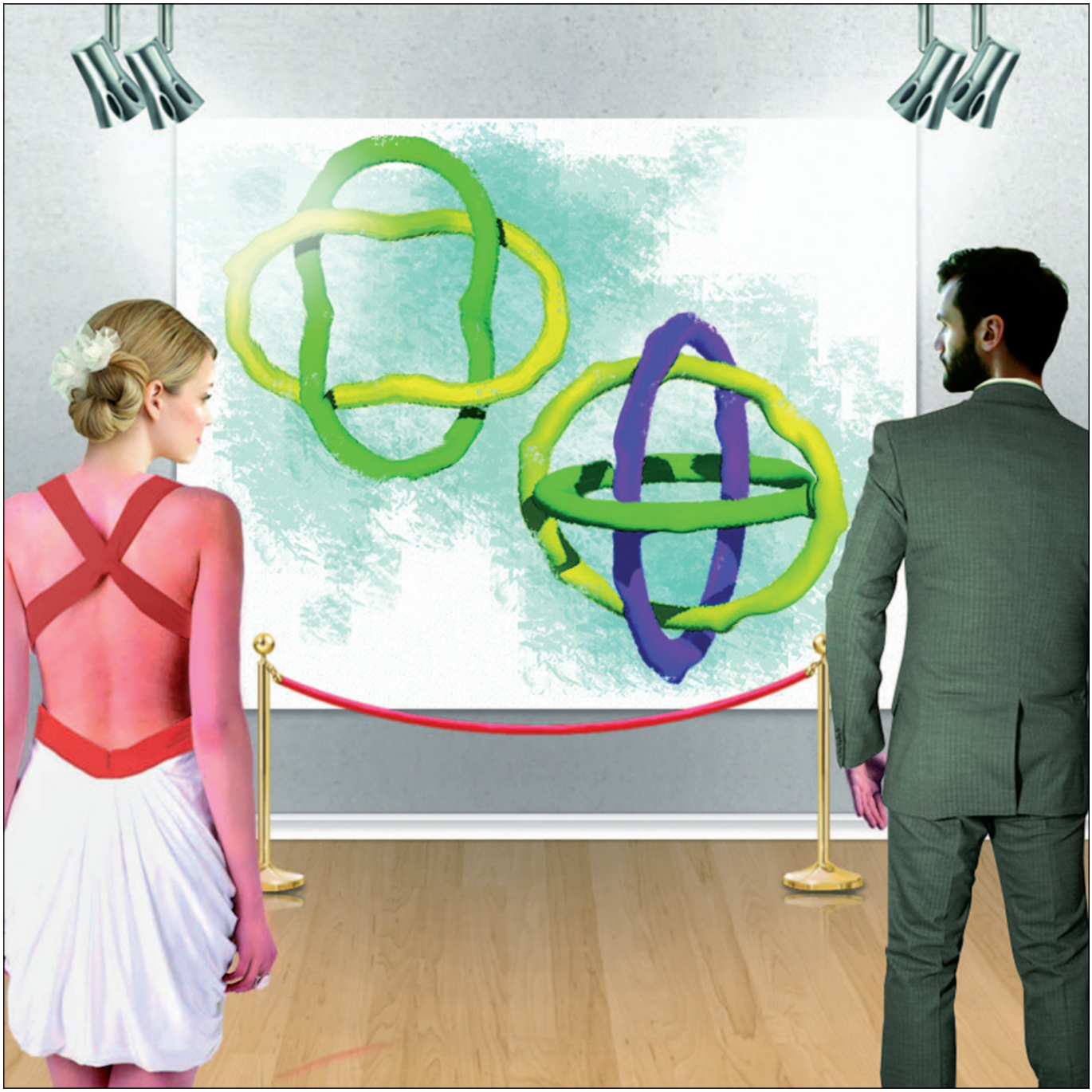

Abstract: The dynamic solution equilibria between molecular Borromean rings (BRs) and Solomon knots (SKs), assembled from transition metal-templated macrocycles, consisting of *exo*-bidentate bipyridyl and *endo*-tridentate diiminopyridyl ligands, have been examined with respect to the choice of the metal template and reaction conditions employed in the synthesis of the metalated BRs, otherwise known as Borromeates. Three new Borromeates, their syntheses templated by Cu^{II}, Co^{II}, and Mn^{II}, have been characterized extensively (two by X-ray crystallography) to the extent that the metal centers in the assemblies have been shown to be distanced sufficiently from each other not to communicate. The solid-state structure of the Co^{II}–Borromeate reveals that six MeOH molecules, arranged in a [O–H···O] hydrogen bonded, chair-like conformation, are located within its oxophilic central cavity. When a mixture of Cu^{II} and Zn^{II} is used as the source of templation, there exists a dynamic equilibrium, in MeOH at room temperature, between a mixed-metal BR and a SK, from which the latter has been fractionally crystallized. By employing appropriate synthetic protocols with Zn^{II} or Cd^{II} as the template, significant amounts of SKs are formed alongside BRs. Modified crystallization conditions resulted in the isolation of both an all-zinc BR and an all-zinc SK, crystals of which can be separated manually, leading to the full characterization of the all-zinc SK by ^{1}H NMR spectroscopy and X-ray crystallography. This doubly interlocked [2]catenate has been identified retrospectively in recorded spectra, where it was attributed previously to a Borromeate with a Zn^{II} cation coordinated to the oxophilic interior walls of the ensemble. Interestingly, these Zn^{II}-templated assemblies do not interconvert in MeOH at room temperature, indicating the significant influence of both the metal template and solvent on the solution equilibria. It would also appear that d^{10} metal ions favor SK formation—no evidence of Cu^{II}-, Co^{II}-, or Mn^{II}-templated SKs has been found, yet a 1:0.9 ratio of BR:SK has been identified by ^{1}H NMR spectroscopy when Cd^{II} is used as the template.

Keywords: coordination compounds · dynamic covalent chemistry · Schiff bases · self-assembly · template-directed synthesis

Introduction

The report by Wasserman[1] in 1960 of the synthesis of a [2]catenane[2] by means of a statistical approach heralded the beginning of the practical expression of chemical topology[3] and topological stereochemistry[4] for the creation of a large collection of mechanically interlocked molecules (MIMs)[5] that rely on the most recent addition to the chemical bond repertoire, the mechanical bond,[6] for their existence. Both kinetically and thermodynamically controlled template-directed reactions,[7] almost always occurring under the direction of noncovalent bonding interactions[8] and increasingly subject to conditions that lead to the formation of dynamic coordinative[9] and covalent[10] bonds, have resulted in good to excellent yields of MIMs, many of which carry functionality wherein mechanical movement can be induced by external stimuli, thus comprising molecular switches or machines.[11]

In the pursuit of ever more complex MIMs, the syntheses of a [5]catenane[12] (Olympiadane) and a branched [7]catenane[13] from a common [3]catenane intermediate were two highlights of an earlier era in our research laboratories at Birmingham University. Thereafter, in response to the desire to take on a substantially more demanding synthetic challenge, a number of members in the group (by that time situated at the University of California, Los Angeles) started working on the task of designing and synthesizing molecular analogues of Solomon knots (SKs) and of Borromean rings (BRs).

The Solomon knot, named so after the wise King Solomon of antiquity, can be described in numerous ways.[14] Mathematically,[15] the nomenclature 'knot' is incorrect. The topology is actually a 'link', more accurately, a 4_1^2 link, comprising, as it does, two components and four crossings. In deference to the rich history of the assembly, we will continue to denote it as a Solomon knot, or SK for short. In chemical topology, SKs have been referred[16] to as 'doubly interlocked' or 'doubly braided' catenanes,[17] and as four-noded links. These four nodes represent a wholly complementary alternating +/–/+/– sequence on each ring (Figure 1a), which can be thought of chemically as *exo*/*endo*/*exo*/*endo* binding sites.

[a] Dr. C. D. Meyer, Dr. K. S. Chichak, Dr. A. J. Peters, N. Tangchaivang, Dr. S. I. Khan, Dr. S. J. Cantrill, Prof. J. F. Stoddart
The California NanoSystems Institute
and Department of Chemistry and Biochemistry
University of California, Los Angeles
405 Hilgard Avenue, Los Angeles, CA 90095-1569 (USA)
Fax: (+1) 310-206-5621
E-mail: stoddart@chem.ucla.edu

[b] Dr. R. S. Forgan, Prof. J. F. Stoddart
Center for the Chemistry of Integrated Systems
and Department of Chemistry, Northwestern University
2145 Sheridan Road, Evanston, IL 60208-3133 (USA)
Fax: (+1) 847-491-1009
E-mail: stoddart@northwestern.edu

[c] Dr. G. W. V. Cave
School of Science and Technology
Nottingham Trent University
Nottingham, NG11 8NS (UK)

Supporting information for this article is available on the WWW under http://dx.doi.org/10.1002/chem.201001806.

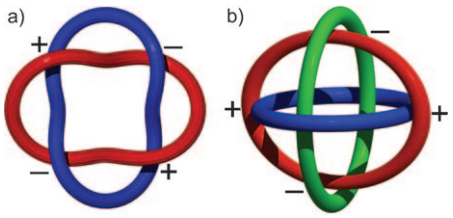

Figure 1. Representations of a) an SK and b) a BR, illustrating the similarity of the alternating +/−/+/− sequences of crossover nodes experienced by each ring constituting their respective assemblies, with the nodal sign annotated for the red ring in each case.

The broad adoption[14] of SKs as a symbol of knowledge and wisdom in myriad cultural settings throughout the ages is rivaled only by that of its interlocked sibling, the Borromean rings (BRs). Named after the Borromeo family of 15th century Italy[18], it is the unique topology[3f,19] of BRs—cut any one of the three rings and the whole cluster falls apart, affording three individual components in the shape of two separated rings and the free linear remnant of the severed ring—that has given them pride of place through the ages in culture[18] as they relate, for example, to mythology, iconography, theology, heraldry, and art in its many different forms, as well as to mathematics,[3e,20] physics,[21] chemistry,[19] and biochemistry.[22] Topologically, six crossover points, or nodes, are present in the BRs, which, when the three rings are represented (Figure 1b) in a three-dimensional, mutually perpendicular manner, manifest themselves as complementary alternating +/−/+/− sequences in a manner strikingly similar to the previously described SK.

Transporting SKs and BRs from Celtic monuments and renaissance heraldry into the molecular world has not been an easy task to tackle or accomplish. Molecular SKs prepared thus far have relied on metal templation. Sauvage et al. have utilized[16a] the helical assembly provided by the Cu^{I} coordination of tris-1,10-phenanthroline ligands to form the four nodes required of a SK followed by appropriate linkage of the threads to complete the assembly. In collaboration with the group of Fujita, a second SK has been prepared by Sauvage using a protocol that exploits the different coordination geometries of both Cu^{I} and Pd^{II}.[16b] Puddephatt et al.[16c] have also realized a molecular SK employing Au^{I} coordination, while Quintela et al.[16d] have called upon donor–acceptor interactions and the dynamic nature of Pd^{II} coordination chemistry to form the link. Pd^{II} chemistry has also made it possible for the group of Hardie[16e] to assemble a related Solomon cube.

Molecular BRs, however, have proven far harder to bring into being. While Borromean linkages have been identified[23] in the extended frameworks of solid-state materials, attempts to prepare truly molecular BRs as single entities have followed two main strategies: 1) the 'ring-in-ring' approach, in which three macrocycles are assembled in a stepwise, linear fashion, and 2) the 'all-in-one' approach, wherein three rings are brought together in a single assembly process.[3f,19] The former strategy has led to the preparation of a number of ring-in-ring complexes[24] composed of one macrocycle threaded through another in a perpendicular fashion, such that the third and final ring can, in principle, be threaded appropriately through the ensemble provided by the first two rings, to form BRs.[25] Although it would seem that assembling the first two macrocycles in the form of a ring-in-ring complex is relatively simple, in our experience[24e,f] threading the third and final one in the appropriate manner is far from easy. A truly orthogonal binding motif has yet to be uncovered, despite a good deal of daring speculation in the literature.[26] Interactions between the two components of the ring-in-ring complex must be suitably strong to hold the assembly together, but not mask the binding sites intended for threading of the final piece of the puzzle.[24f] Quite a tall order, yet one day someone will find a way to carry it out.

While the stepwise ring-in-ring approach under kinetic control offers access to more constitutional diversity, the all-in-one strategy under thermodynamic control is particularly suited to the assembly of complex architectures. The elegant manipulation[22] of DNA strands, perhaps the ultimate supramolecular synthons, by the group of Seeman brought molecular BRs into being by ligating a right-handed B-DNA three-arm junction with a left-handed Z-DNA three-arm junction through this all-in-one approach. Subsequently, it was also shown that three different enzymes could cleave, in separate experiments, the three individual rings of 196, 206, and 216 nucleotides in the BR compound comprised of DNA. The consequence of cleaving any one ring was shown, by gel electrophoresis, to lead to the release of the other two rings as separate entities—an elegant demonstration of the BR topology.

In focusing our attempts to prepare molecular BRs through an all-in-one strategy, we have designed,[27] with the aid of computational calculations, a retrosynthetic strategy wherein the six nodes that represent the crossing points of the rings are endowed with the directional templation inherent to transition-metal cations. Namely, a compound, wherein three identical macrocycles present, diagonally in pairs, six *exo*-bidentate bipyridyl and six *endo*-tridentate diiminopyridyl ligands to six divalent metal cations, was designed to take advantage of the combined forces of noncovalent,[8] coordination,[9] and dynamic covalent[10] chemistry; this endows the self-assembly process simultaneously with directionality, error checking, and reversibility. When Zn^{II} was used[28] as the templating transition-metal ion, it proved possible to prepare the molecular BR, $Zn^{II}BR{\cdot}12\,TFA$ (TFA = trifluoroacetate; Figure 2), in a highly efficient (≈95% yield) manner. Herein, we report the production of a series of molecular BRs, templated by various transition-metal dications, by multiply cooperative self-assembly processes. The serendipitous discovery of related molecular SKs,[29] and the interplay between these SKs and BRs in solution and the solid state will also be a subject for discussion.

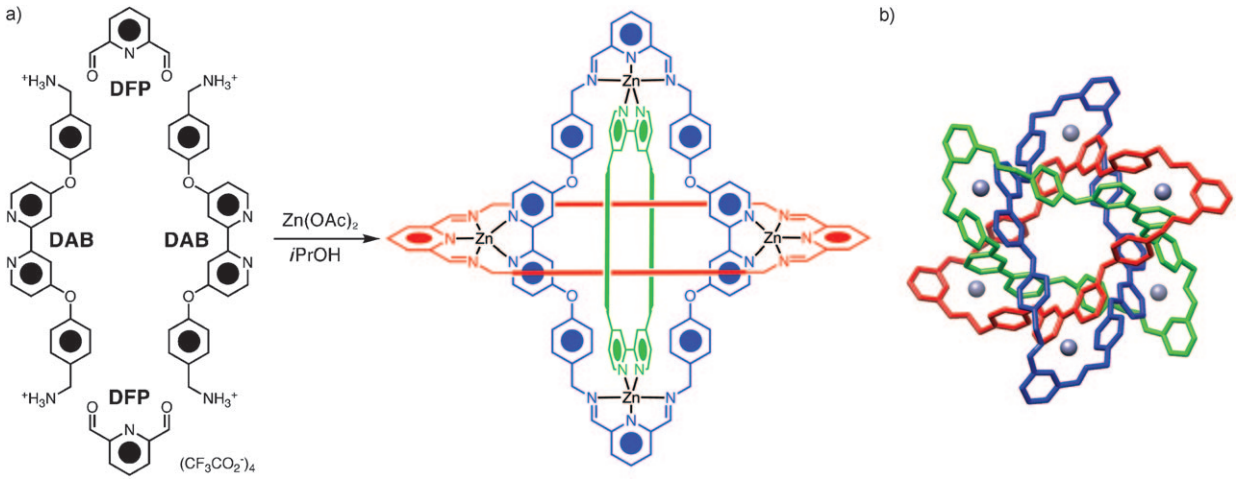

Figure 2. a) Synthesis of $Zn^{II}BR^{12+}$ from $Zn(OAc)_2$, diformylpyridine (DFP), and the diaminobipyridine (DAB) compound, which is generated in situ from its *tert*-butyloxycarbonyl (Boc)-protected precursor (Boc-DAB) by deprotection with trifluoroacetic acid. b) The solid-state structure of the $Zn^{II}BR^{12+}$ dodecacation, with each individual ring colored red, blue, and green. Hydrogen atoms, solvents, and counterions removed for clarity and generated from CCDC deposition 231701.

Results and Discussion

Pleased with our initial success in preparing $Zn^{II}BR{\cdot}12\,TFA$, we sought to extend the series of Borromeates[30] by employing alternative metal cations as templates. The first-row transition metals are clear choices, bearing in mind the necessity for the templating metal ion to form octahedral coordination complexes and also be sufficiently kinetically labile to permit reversibility and error checking to occur in the 18-component self-assembly process. It has proven possible to prepare the compounds listed in Table 1 by careful control of reaction temperature, time, and solvent conditions. $Cu^{II}BR{\cdot}12\,TFA$, $Co^{II}BR{\cdot}12\,TFA$, and $Mn^{II}BR{\cdot}12\,TFA$ could be purified by recrystallization,[32] although purification and characterization of $Cd^{II}BR{\cdot}12\,TFA$ was complicated, and will be discussed separately in more detail later.

Single crystals, suitable for X-ray crystallography, of $Cu^{II}BR{\cdot}12\,TFA$ were grown by layer diffusion of Et_2O into a solution of the compound in methanol. X-ray crystallographic analysis,[33] carried out on a single crystal,[34] reveals that the molecular structure of $Cu^{II}BR{\cdot}12\,TFA$ has the Borromean topology (Figure 3) with the three rings interlocked in the Brunnian manner. Each of the three rings adopts a chair-like conformation and the molecule, which has S_6 symmetry, is isostructural with the previously reported $Zn^{II}BR{\cdot}12\,TFA$.[27] The three rings, 25.0 Å from apex to apex, are held in place by six hexacoordinate Cu^{II} ions, which occupy the vertices of an octahedron that is facially compressed through the principal S_6 axis of symmetry (Figure 3a). The Cu^{II} ions, which occupy the two planes that make up the upper and lower faces of this octahedron, are separated by 12.7 Å and the remaining six edges joining the two faces are 12.5 Å in length. The copper centers are octahedral (Figure 3b), each bound to five nitrogen atoms and one oxygen atom. There exists a significant tetragonal elongation, in keeping with a Jahn–Teller effect, in the bonds between the Cu^{II} cation and the two imine nitrogen atoms of the complex, N1 and N3. The remaining four coordination sites are occupied by the pyridyl nitrogen atom (N2), the two bipyridyl nitrogen atoms (N4 and N5) and a distorted trifluoroacetate counterion by means of an η^1 coordination to one of the oxygen atoms (O3).

Alongside the cooperativity displayed by these six Cu^{II} ions in holding the three individual rings together, the

Table 1. Synthetic conditions employed in the preparation of BRs by using a range of divalent transition metal cation templates, alongside characteristic signals seen in their respective mass spectra.

	Solvent	T [°C]	t [h]	Yield [%]	ESI-MS signals $[m/z]$[a]
$Zn^{II}BR^{12+}$[b]	*i*PrOH	70	24	95	1465.1902 $[M-3\,TFA]^{3+}$, 1070.1398 $[M-4\,TFA]^{4+}$, 833.7088 $[M-5\,TFA]^{5+}$
$Cu^{II}BR^{12+}$	*i*PrOH	70	72	85	2248.2996 $[M-2\,TFA]^{2+}$, 1461.2580 $[M-3\,TFA]^{3+}$, 1067.6730 $[M-4\,TFA]^{4+}$, 831.5383 $[M-5\,TFA]^{5+}$
$Co^{II}BR^{12+}$	MeOH	65	96	36	2234.5859 $[M-2\,TFA]^{2+}$, 1451.9632 $[M-3\,TFA]^{3+}$, 1060.6455 $[M-4\,TFA]^{4+}$, 1765.2038 $[2M-5\,TFA]^{5+}$[c]
$Mn^{II}BR^{12+}$	*i*PrOH	70	72	70	1443.9618 $[M-3\,TFA]^{3+}$, 1054.7134 $[M-4\,TFA]^{4+}$, 821.1094 $[M-5\,TFA]^{5+}$
$Cd^{II}BR^{12+}$	*i*PrOH	65	12	80	1588.1758 $[M-3\,TFA]^{3+}$, 1141.1369 $[M-4\,TFA]^{4+}$

[a] Electrospray mass spectra were collected on crystalline samples redissolved in MeOH, except in the case of $Cd^{II}BR^{12+}$, in which a crude sample was used. [b] Data taken from ref. [28]. [c] While this peak most likely occurs as a result of gas-phase dimerization of $Co^{II}BR^{12+}$, we have also considered the possibility that this larger mass signal is a result of a so-called 'big BR' or other larger interlocked molecules that formed as a minor product in the synthesis of $Co^{II}BR^{12+}$. Using Spartan and CPK models, we have determined that it would not be impossible for a 'Big BR' to form in which 12 DFP units and 12 DAB units, and 12 Co^{II} metal ions come together to form an assembly of three large macrocycles.

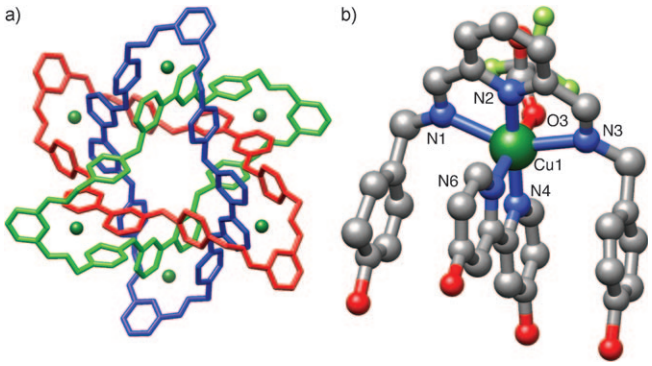

Figure 3. The solid-state structure of $Cu^{II}BR{\cdot}12\,TFA$. a) Tubular representation viewed down the S_6 axis of the three interlocked rings colored red, blue, and green, with the Cu^{II} atoms colored a metallic green, where the distance from apex to apex is 25.0 Å. The central pore of 2.0 Å in diameter allows access into an inner cavity of 329 $Å^3$. b) Ball-and-stick representation of one of the six identical six-coordinate copper(II) centers of $Cu^{II}BR^{12+}$, which is bound by five nitrogen atoms and an oxygen from a trifluoroacetate anion. Selected bond lengths: Cu1–O3 = 1.98(1), Cu1–N1 = 2.40(1), Cu1–N2 = 2.03(1), Cu1–N3 = 2.36(1), Cu1–N4 = 1.98(1), Cu1–N5 = 2.03(1) Å. Hydrogen atoms and disorder in the trifluoroacetate anions have been omitted for clarity.

$Cu^{II}BR^{12+}$ ions are further stabilized by the grasping actions of the flanking phenyl rings, which pinch the six bipyridyl ligands by means of 12 π–π stacking interactions, with centroid distances of 3.73 and 3.88 Å from the two carbon atoms of the 2,2′-bipyridyl bond. The organic layer of $Cu^{II}BR^{12+}$ encapsulates an inner cavity of 329 $Å^3$, which can be accessed through 2.0 Å pores located about the S_6 axis of symmetry. The $Cu^{II}BR^{12+}$ ions are arranged in a close-packed ABC hexagonal array (see below). The distance between the centers of each $Cu^{II}BR^{12+}$ ion in the hexagonal planes is 34.1 Å along the *a* and *b* axis of the unit cell and 7.4 Å between the hexagonal planes. The rings are significantly interdigitated and compacted together, with the interstitial voids filled with a single MeOH molecule that is disordered over two sites, and trifluoroacetate counterions, which balance the charge of the dodecacationic $Co^{II}BR{\cdot}12\,TFA$ complex.

Single crystals[35] of $Co^{II}BR^{12+}$, suitable for X-ray crystallography, were grown by vapor diffusion of Et_2O into a solution of $Co^{II}BR^{12+}$ in methanol. X-ray crystallographic analysis of a single crystal of $Co^{II}BR^{12+}$ afforded a structure (Figure 4) that is similar to that of the solid-state structure of $Cu^{II}BR^{12+}$ with respect to the manner in which the three rings are interlocked.

There is, however, one major difference in the structure of the $Co^{II}BR^{12+}$ dodecacation (Figure 4a). Disorder exists, such that one of the rings occupies two different chair conformations (1:1 ratio), resulting in the presence of two molecular trinities, one with C_i symmetry and the other with S_6 symmetry. This observation is consistent with the findings of molecular modeling studies that were performed[27] initially on the topology during the design of the BRs, where it was revealed that the energy difference ($\Delta E = 2$ kcal mol^{-1}) between the two structures was very small. The three rings, 26.0 Å from apex to apex, are held in place by six Co^{II} ions that also occupy the vertices of an octahedron. The distances between neighboring Co^{II} atoms (or edges of the octahedron) range from 12.6 to 13.1 Å with the average distance calculated as 12.9 Å.

Although the volume of the inner cavity of the $Co^{II}BR^{12+}$ ion is 250 $Å^3$, similar to that found for the original zinc-containing BRs,[27] the cavity in $Co^{II}BR^{12+}$ contains six hydrogen-bonded molecules of MeOH arranged in a chair conformation (Figure 4b–d). The molecular volume of the six MeOH molecules inside the BR cavity is 209 $Å^3$, which results in a packing efficiency inside the cavity of 84 %.[36] The packing diagram (Figure 5) of $Co^{II}BR^{12+}$ shows that the ions are arranged as a layered pseudo-hexagonal array. The distance between the centers of each $Co^{II}BR^{12+}$ ion is the same as the unit cell dimensions ($a = 19.46(1)$, $b = 20.32(1)$, $c = 22.62(1)$ Å). Of the 12 trifluoroacetate anions that are expected to accompany the $Co^{II}BR^{12+}$ dodecacation, only the six that are bonded to the Co^{II} cations were resolved. The remaining six outer-sphere counterions could not be resolved.

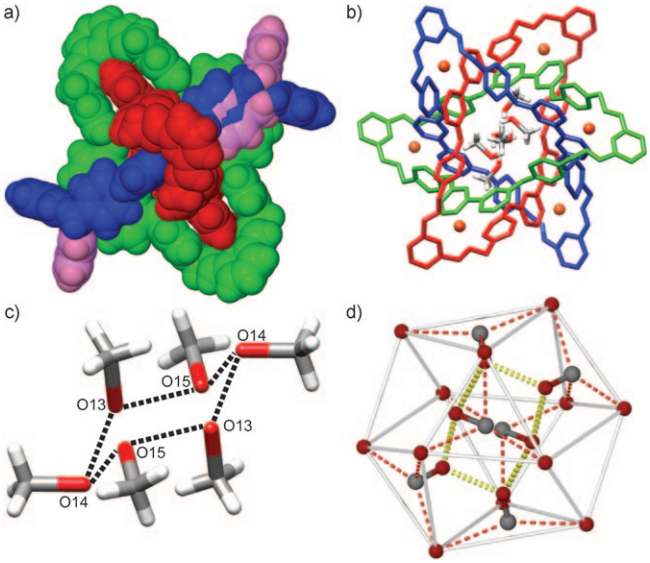

Figure 4. The solid-state structure of $Co^{II}BR{\cdot}12\,TFA$. Individual $Co^{II}BR^{12+}$ complexes are shown as tubular and space-filling representations with the three equivalent rings colored red, blue, and green and the Co^{II} atoms colored orange. Hydrogen atoms, counterions, solvents, and disorder have been removed for clarity unless mentioned. a) Space-filling representation of $Co^{II}BR^{12+}$, illustrating the disorder of one of the three macrocycles, forming a 1:1 ratio of $Co^{II}BR^{12+}$ dodecacations with S_6 symmetry (blue macrocycle) and C_i symmetry (pink macrocycle) The isomers become isostructural at the C69 alkene and O5 ether linkage, and share a common axial point at the N13 imine atom. Hydrogen atoms have been omitted for clarity. b) A tubular representation of the S_6 isomer containing six highly ordered MeOH solvent molecules in the central cavity. c) The 'chair conformation' defined by six hydrogen-bonded MeOH molecules found in the central cavity of $Co^{II}BR^{12+}$, O···O = 2.48–2.71 Å. d) View of the MeOH molecules and the surrounding icosahedron of ether O atoms at the center of $Co^{II}BR^{12+}$. The methanolic C atoms are positioned at each of the triangular faces of the icosahedron. Four of the MeOH molecules have their Me groups aligned equatorially and two axially about the hydrogen-bonded cluster, allowing them to each hydrogen bond to three of the $Co^{II}BR^{12+}$ ether linkages (C···O = 2.98–3.59 Å).

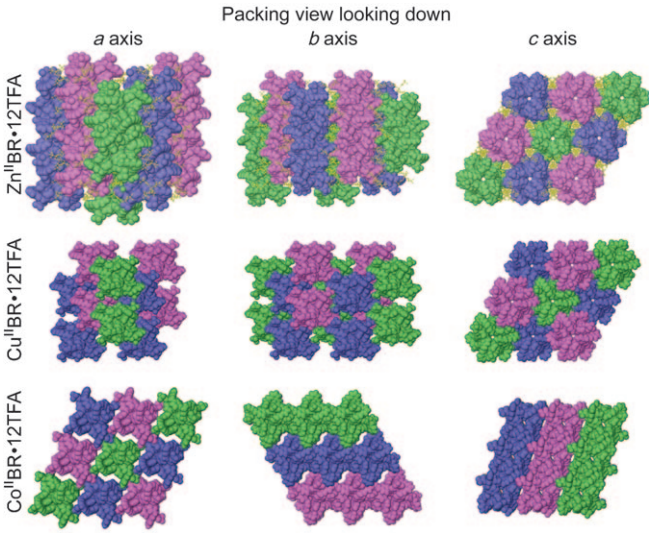

Figure 5. Comparison of the packing diagrams of $Zn^{II}BR{\cdot}12TFA$[26] (top row), $Cu^{II}BR{\cdot}12TFA$ (middle row), and $Co^{II}BR{\cdot}12TFA$ (bottom row) when viewed down the *a*, *b*, and *c* crystallographic axes. Hydrogen atoms, counterions, and solvent are removed for clarity, except in the case of $Zn^{II}BR{\cdot}12TFA$ where counterions are shown in yellow.

Comparison of the molecular packing diagrams of the three BRs, $Zn^{II}BR{\cdot}12TFA$, $Cu^{II}BR{\cdot}12TFA$, and $Co^{II}BR{\cdot}12TFA$ (Figure 5) reveals three unique structures. The $Co^{II}BR^{12+}$ (shown as a single conformation) packing diagrams reveal that the structure contains extensive interconnected channels running though the *a* and *b* axes (100 and 010). The channels contain disordered solvent molecules and trifluoroacetate counterions.

Since the Borromeates templated by Cu^{II}, Co^{II}, and Mn^{II} are all paramagnetic, it should be possible to characterize them by EPR spectroscopy. The X-band EPR spectrum (see the Supporting Information) of $Cu^{II}BR^{12+}$ displays characteristic axial symmetry with a $g_{II} > g_{\perp}$ tensor pattern that is typical of a tetragonally elongated $d_{x^2-y^2}$ ground state for Cu^{II}, which has been observed[37] in similar complexes and is commensurate with the solid-state structure of $Cu^{II}BR{\cdot}12TFA$. The spectrum is indicative of having six isolated Cu^{II} atoms, the magnetic spins of which are distanced sufficiently far from each other within the framework of $Cu^{II}BR{\cdot}12TFA$ such that they do not communicate. The X-band EPR studies on a sample of $Co^{II}BR^{12+}$ were performed at 4 K, and the spectrum (see the Supporting Information) shows one broad signal with a *g* factor of 3.94. The X-band EPR spectrum (see the Supporting Information) of $Mn^{II}BR^{12+}$ shows five distinct nondegenerate electronic transitions as a result of the five unpaired electrons present in high-spin Mn^{II} nuclei. The EPR spectra of the three Borromeates suggest that the metal cations are degenerate and do not communicate with each other, a thesis that is supported by cyclic voltammetry (CV) experiments carried out in anhydrous DMF (see the Supporting Information). The cyclic voltammogram of $Cu^{II}BR{\cdot}12TFA$ shows a quasi-reversible reduction peak at -0.39 V, expected for a Cu^{II}/Cu^{I} redox couple, with the expected cathodic peak for the Cu^{I}/Cu^{II} redox couple appearing at $+0.06$ V. Two redox waves can be identified in the CV of $Co^{II}BR{\cdot}12TFA$: 1) a quasi-reversible redox wave at $+0.42$ V arising from the Co^{II}/Co^{III} redox couple, and 2) a reversible wave at -0.67 V arising from the Co^{II}/Co^{I} redox couple. The CV of $Mn^{II}BR{\cdot}12TFA$ shows a quasi-reversible reduction peak at -1.04 V, with the cathodic peak appearing at -0.95 V, ascribable to the Mn^{II}/Mn^{III} redox couple. In each case, the presence of single peaks for each redox couple indicates yet again that the metal cations are sufficiently distanced from each other to behave independently.

Purification and characterization of the crude products from a Cd^{II}-templated synthesis was not straightforward, since no crystallization protocol was discovered. Since Cd^{II} is diamagnetic, the crude powder isolated in the synthesis of $Cd^{II}BR{\cdot}12TFA$ was examined by ^{1}H NMR spectroscopy, revealing two distinct sets of peaks and suggesting that another symmetric product is present along with the Cd–Borromeate. Similarly, the high-resolution (HR) ESI mass spectrum (see the Supporting Information) of the crude powder containing $Cd^{II}BR{\cdot}12TFA$ dissolved in MeOH revealed, not only a pair of peaks at *m*/*z* 1588.1758 $[M-3TFA]^{3+}$ and 1141.1369 $[M-4TFA]^{4+}$, but also a pair of peaks at *m*/*z* 1588.1758 (superimposed on the molecular ion peak) and 1001.7761 corresponding to a compound with approximately two thirds of the mass of the BR derivative. Similarly, while under appropriate[38] conditions (see Table 1), $Zn^{II}BR{\cdot}12TFA$ can be isolated[28] in yields of 95%, even when the reaction is conducted[39] on a gram scale, the crude powder obtained from the reaction will often contain[27] a minor product that can be detected by ^{1}H NMR spectroscopy as well as by mass spectrometry. Originally, we hypothesized[27] that the second set of signals observed in the ^{1}H NMR spectrum resulted from a BR species, in which a seventh zinc ion had found its way into its oxophilic cavity, affording $Zn@Zn^{II}BR{\cdot}12TFA$, a supposition that was also supported by the appearance of appropriate signals in the mass spectrum. However, this second species proved elusive. By employing the original crystallization protocol, in which only $Zn^{II}BR{\cdot}12TFA$ crystallizes, the minor product could not be isolated, despite repeated attempts.

The possible identity of this mysterious side product was revealed[29] during an investigation into the effects of using mixed-metal templates in the self-assembly of molecular BRs. When equimolar quantities of Cu^{II} and Zn^{II} were utilized as templates in the attempted synthesis of $Cu^{II}/Zn^{II}BR{\cdot}12TFA$, green crystals suitable for X-ray diffraction analysis were isolated by $MeOH/Et_2O$ vapor diffusion. They were shown by X-ray crystallographic analysis to constitute a molecular SK, $Cu^{II}/Zn^{II}SK{\cdot}8TFA$, wherein two macrocycles are doubly interlocked and templated by four metal cations. ESI-MS recorded on solutions of redissolved crystals in methanol revealed signals, not only for the mixed-metal SK product, but also for the mixed-metal Borromeate, $Cu^{II}/Zn^{II}BR{\cdot}12TFA$. It follows that the mixed-metal SK and BR assemblies are interconverting in solution, by means of dy-

namic coordinative chemistry and the reversible imine bond, generating a dynamic library of species from which Cu^{II}/Zn^{II}SK·8TFA can be crystallized selectively, under kinetic control.

Intrigued by the possibility of an all-Zn SK and an all-Cd SK being the side products visible in the ^{1}H NMR spectrum and ESI mass spectrum of the respective crude products, we pursued these species by attempting to crystallize[40,41] Zn^{II}SK·8TFA and Cd^{II}SK·8TFA selectively in preference to their respective BR siblings. While we were unable to isolate crystals of any Cd^{II}-containing species, when Et_2O was vapor diffused into a *n*PrOH/MeOH (3:1) solution of the crude reaction product that contained a 4:1 mixture of Zn^{II}BR·12TFA and the impurity identified previously by ^{1}H NMR spectroscopy, two distinct sets of crystals separated (Figure 6a), one as long colorless needles and the other as small colorless octahedra. The first set of crystals resembled the familiar[27] needle-shaped ones of Zn^{II}BR·12TFA, and X-ray crystallographic analysis of one of these single crystals confirmed that the molecular structure did indeed correspond to the Borromean topology, and the data match precisely the previously obtained X-ray crystallographic data for Zn^{II}BR·12TFA.[27] X-ray crystallographic analysis[42] of the second set of octahedral crystals revealed that these crystals are the result of the crystallization of a new molecular species, Zn^{II}SK·8TFA, from the reaction medium.

The solid-state structure of Zn^{II}SK·8TFA represents a crystalline racemate[43] of the *P* and *M* enantiomers,[4b] as indicated by the enantiomeric pair (Figure 6b) of molecules present in the unit cell (Figure 6c). The four equivalent Zn^{II} metal ions of the cluster are arranged in an approximately square fashion with adjacent M–M distances of 11.3 and 11.9 Å, whereas the two diagonally opposing Zn atoms are

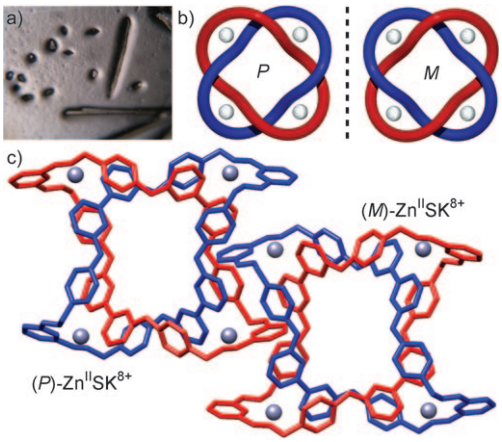

Figure 6. a) Octahedral crystals of Zn^{II}SK·8TFA (left) alongside needle-like crystals of Zn^{II}BR·12TFA (right) resulting from recrystallization of the crude material by vapor diffusion of Et_2O into a 3:1 solution of *n*PrOH/MeOH. b) Schematic diagram of the *P* and *M* enantiomers possible in the SK topology (4_1^2). c) The solid-state structure of Zn^{II}SK·8TFA, illustrating both the *P* and *M* enantiomers present in the unit cell. Hydrogen atoms, counterions, solvent, and disorder removed for clarity, each independent ring colored red and blue, Zn^{II} cations represented as silver spheres.

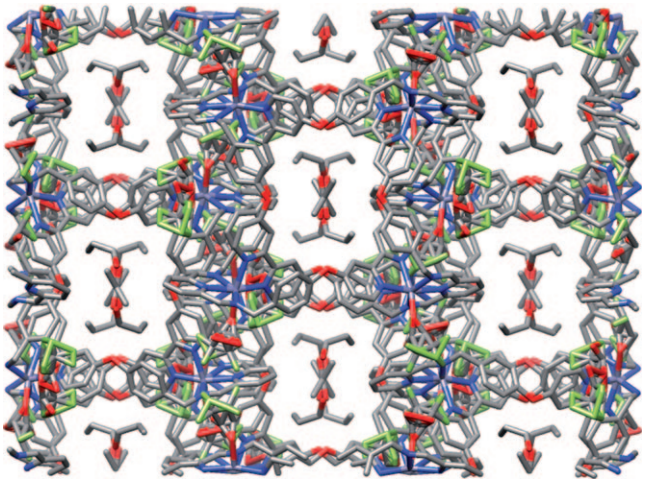

Figure 7. Packing diagram of Zn^{II}SK·8TFA viewed down the *b* axis. The pores visible at the centers of the aligned $Zn^{II}SK^{8+}$ octacations contain disordered solvent molecules. Hydrogen atoms removed for clarity.

located 16.4 Å apart. Through the center of this cavity lie two mutually perpendicular twofold crystallographic axes, such that all four metal sites are equivalent. Each Zn^{II} cation has a distorted octahedral geometry, with bonds to five N atoms of the two macrocyclic ligands (M–N bond lengths range from 2.11 to 2.26 Å and *cis* N-M–N bond angles ranging from 73.4 to 117.0°) with the final coordination site occupied by the oxygen atom of a disordered trifluoromethyl group (M–O bond length of 2.05 Å and bond angles ranging from 87.5 to 99.4°). Each bipyridyl ligand lies between a pair of benzyloxy rings with π–π stacking distances of 3.8 and 3.9 Å.

All eight oxygen atoms of the two macrocycles point inwards into the central cavity in a distorted cubic array. The three adjacent O···O distances from each corner of this cube are 5.7, 5.7, and 4.3 Å. The cavity is filled (Figure 7) with disordered solvent molecules (*n*PrOH and/or MeOH). Since the disorder is extensive, plus the fact that this site has imposed crystallographic symmetry, it was not possible to distinguish crystallographically which one of these two solvents occupies the core of Zn^{II}SK·8TFA. The length of the cavity (4.3 Å) along the long direction of the disordered solvent suggests that *n*PrOH would fit most appropriately.

Other than for solvent differences, the packing diagram of Zn^{II}SK·8TFA is noticeably similar to its mixed-metal analogue, Cu^{II}/Zn^{II}SK·8TFA. The interstitial sites between each Zn^{II}SK·8TFA are filled with solvent molecules, which, although disordered, could be consistent with the structure of *n*PrOH. Considering that the solvent is the only known variable that was changed during the crystallization conditions leading up to the isolation of crystals of Zn^{II}SK·8TFA, their participation in the packing of the molecular SK^{8+} is not unexpected.

The octahedral crystals, obtained using the modified crystallization conditions, were isolated by hand, and the ^{1}H NMR spectrum (Figure 8) revealed, without a doubt, that the previously overlooked 'minor' product[44] is

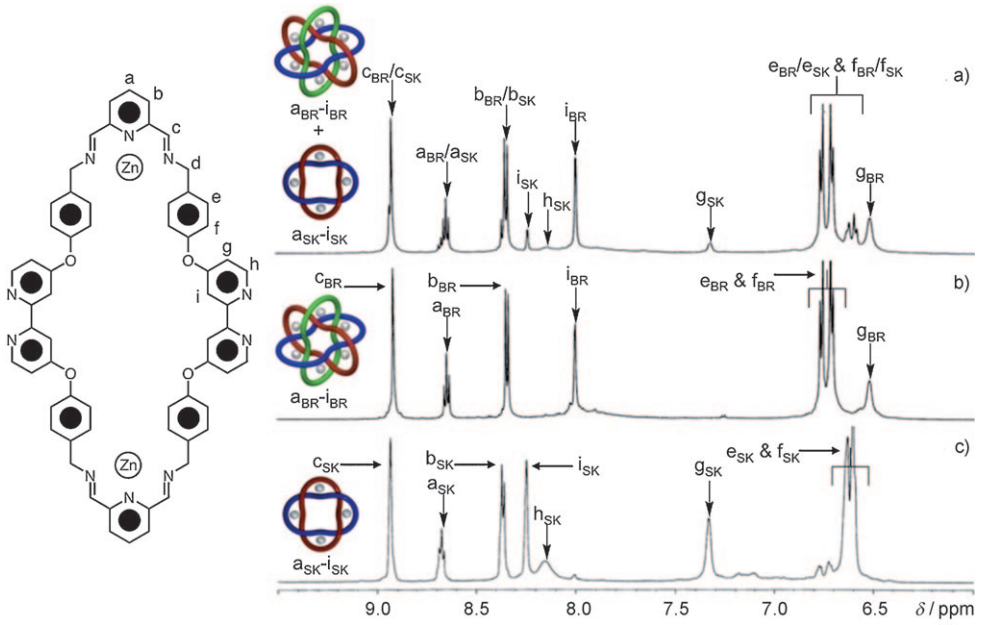

Figure 8. ^{1}H NMR spectra (600 MHz, MeOD, 298 K), with assignments for a) the crude reaction mixture, containing $Zn^{II}BR{\cdot}12\,TFA$ and $Zn^{II}SK{\cdot}8\,TFA$ present in a 4:1 ratio, respectively; b) the isolated needlelike crystals of $Zn^{II}BR{\cdot}12\,TFA$; and c) the isolated octahedral crystals of $Zn^{II}SK{\cdot}8\,TFA$.

$Zn^{II}SK^{8+}$ and not $Zn@Zn^{II}BR^{12+}$. The assignment[45] of the SK^{8+} signals represents the first time we have been successful in performing an ^{1}H NMR spectroscopic analysis, since the Cu^{II} cations in $Cu^{II}/Zn^{II}SK{\cdot}8\,TFA$ presented a roadblock[46] to obtaining an interpretable ^{1}H NMR spectrum. We note that overall the $Zn^{II}SK^{8+}$ peaks are shifted downfield relative to those of $Zn^{II}BR^{12+}$, most evidently for the peaks corresponding to the protons (labeled i_{SK} and g_{SK}) closest to the cavities in each macrocycle: they are shifted downfield by 0.2 and 0.8 ppm, respectively.

In retrospect, these changes in chemical shift make perfect sense. It is the regions of the cavities that are most influenced by the structural differences between the SK^{8+} and BR^{12+} architectures that show the largest downfield shift, in contrast with the peripheral protons, c_{SK}, b_{SK}, and a_{SK}, which overlap with the peaks for $Zn^{II}BR{\cdot}12\,TFA$, or at least are only shifted enough to be observable as shoulders in ^{1}H NMR spectra recorded at 600 MHz. Direct integration of the signals in the ^{1}H NMR spectrum (Figure 8a) of the crude reaction product reveals that $Zn^{II}BR{\cdot}12\,TFA$ and $Zn^{II}SK{\cdot}8\,TFA$ are present in a 4:1 ratio in MeOD at room temperature, and both species can be identified in the ESI mass spectrum (see the Supporting Information).

The conditions employed in this synthesis (*i*PrOH, 60 °C, 32 h) favor the assembly of a significant amount of $Zn^{II}SK{\cdot}8\,TFA$ alongside $Zn^{II}BR{\cdot}12\,TFA$, and, even at room temperature in MeOH, the two species do not interconvert. Unlike the mixed-metal[29] $Cu^{II}/Zn^{II}SK{\cdot}8\,TFA$, the homo-metal $Zn^{II}SK{\cdot}8\,TFA$ persisted in methanol for 34 days. Likewise, the isolated needles of $Zn^{II}BR{\cdot}12\,TFA$ appear to be equally robust in MeOH; the mass spectrum reveals only signals corresponding to the BR species after 34 days. This seemingly minor variation on moving from a mixed Cu^{II}/Zn^{II} system to a Zn^{II}-only system has induced significant changes in the solution equilibria and hindered the interconversion between the two interlocked species—a clear illustration of the complexity of the situation.

Having definitively characterized $Zn^{II}SK{\cdot}8\,TFA$ by ^{1}H NMR spectroscopy, we were able to identify the second set of signals in the ^{1}H NMR spectrum (Figure 9) of the Cd-templated reaction as $Cd^{II}SK{\cdot}8\,TFA$. By comparison of integrals for resonances associated with $Cd^{II}BR{\cdot}12\,TFA$ and $Cd^{II}SK{\cdot}8\,TFA$, it was ascertained that the two species were present in solution in a 1.0:0.9 ratio. Although this ratio corresponds to the highest yield of single-metal SKs prepared to date, it has not proven possible to separate either species

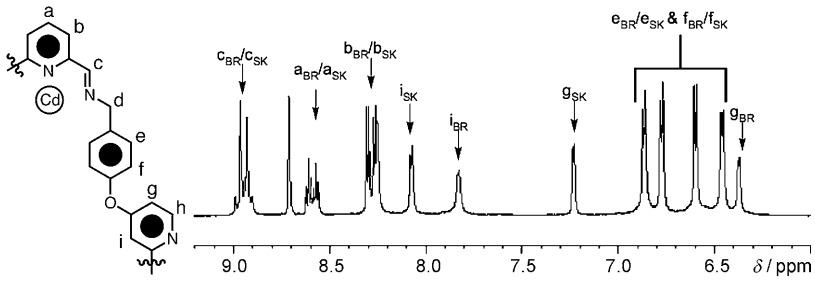

Figure 9. ^{1}H NMR spectrum (600 MHz, 298 K) of the powdered mixture containing $Cd^{II}BR{\cdot}12\,TFA$ and $Cd^{II}SK{\cdot}8\,TFA$, which are present in a 1.0:0.9 ratio, respectively.

by crystallization. Retrospective analysis of the ESI mass spectrum (see the Supporting Information) of the crude powder also showed significant peaks attributable to $Cd^{II}SK{\cdot}8\,TFA$.

Conclusion

It is clear that in this dynamic system the interplay in solution between molecular SKs and BRs is a complicated affair, with many equilibria seemingly affected by the choice of metal cation template and solvent, and control over crystallization of molecular assemblies can be exercized by selecting appropriate crystallization conditions. While utilizing a series of divalent transition-metal cations as templates has led to the characterization of additional Borromeates, mixed-metal templates have allowed isolation of a SK from a dynamic library in solution.[31] It would appear that divalent metal cations with a d^{10} electronic configuration, in particular, induce SK formation. $Zn^{II}SK{\cdot}8\,TFA$ has been isolated by a modified crystallization protocol and definitively characterized by ^1H NMR spectroscopy, subsequently allowing the identification of $Cd^{II}SK{\cdot}8\,TFA$ as part of a crude solution mixture with $Cd^{II}BR{\cdot}12\,TFA$. We can only speculate upon the forces that drive the equilibria between BRs, SKs, and possibly larger, more complex assemblies in solution. At the same time, we can attempt to take advantage of solvent effects during crystallization to isolate different species in the solid-state. Our long relationship with this system has proven fruitful and thought-provoking, and we believe it will yield more surprises as well as a few conundrums in the years to come.

Experimental Section

General: The Boc-protected diaminobipyridine precursor (Boc-DAB) and DFP were prepared as described previously.[25] All solvents were dried prior to use according to literature procedures. UV/Vis spectra were recorded at room temperature on a Varian Cary 100 Bio UV/Vis spectrophotometer. Electrochemical data was collected on a PAR 263A potentiostat/galvonostat interfaced with a PC. A glassy carbon working electrode, silver wire reference electrode, and an isolated platinum wire counter electrode were used in the conventional three-electrode cell. Tetrabutylammonium trifluoracetate (0.1 M) was employed as the supporting electrolyte. Deuterated solvents (Cambridge Isotope Laboratories) for NMR spectroscopic analyses were used as received. All ^1H and ^{13}C NMR spectra were recorded on either a Bruker Avance600 (600 and 150 MHz, respectively), Bruker Avance500 (500 and 125 MHz, respectively), or Bruker ARX500 (500 and 125 MHz, respectively). All chemical shifts are quoted in ppm, relative to tetramethylsilane, using the residual solvent peak as a reference standard. X-band EPR spectroscopic measurements were recorded on a Bruker EMX spectrometer. Mass spectra were measured on an IonSpec 7.0T Ultima FTMS with MALDI and ESI ion sources. MALDI-TOF mass spectra were obtained by using dihydroxybenzoic acid as the supporting matrix. Electrospray mass spectra were obtained with either MeOH or MeCN as the liquid carrier.

$Cu^{II}BR{\cdot}12\,TFA$: Boc-DAB (329 mg, 0.549 mmol) was dissolved in trifluoroacetic acid (2 mL) and stirred at room temperature for 10 min. Excess trifluoroacetic acid was removed by rotary evaporation under reduced pressure, followed by subsequent additions and removals of MeOH (3×5 mL), leaving a pink tar containing DAB-$H_4{\cdot}4\,TFA$. $Cu(OAc)_2$ (103 mg, 0.549 mmol) was added to a stirred solution of *i*PrOH (5 mL) containing freshly deprotected DAB-$H_4{\cdot}4\,TFA$ and DFP (74.2 mg, 0.549 mmol). The reaction mixture was heated at 70 °C for 72 h, producing a green-colored precipitate, which was removed by filtration, washed with *i*PrOH, and Et_2O, and then dried to afford a green powder (368 mg, 85 %). The product was crystallized from a solution in MeOH (2 mL) into which Et_2O was allowed to diffuse slowly. UV/Vis (MeOH, 2.37×10^{-6} M): λ_{max} ($\log\varepsilon$) = 231 (5.44), 293 (4.90), 303 (4.87), 319 nm sh; UV/Vis (MeOH, 5.57×10^{-4} M): λ_{max} ($\log\varepsilon$) = 706 nm (2.18); HRMS (ESI): *m*/*z* (%): 2248.2996 (1) $[M-2CF_3CO_2]^{2+}$, 1461.2580 (80) $[M-3CF_3CO_2]^{3+}$, 1067.6730 (100) $[M-4CF_3CO_2]^{4+}$, 831.5383 (40) $[M-5CF_3CO_2]^{5+}$

$Co^{II}BR{\cdot}12\,TFA$: Boc-DAB (246.3 mg, 0.41 mmol) was dissolved in trifluoroacetic acid (2 mL) and stirred at room temperature for 15 min. Excess trifluoroacetic acid was removed by rotary evaporation under reduced pressure, followed by subsequent additions and removals of MeOH (3×5 mL), leaving a pink tar containing DAB-$H_4{\cdot}4\,TFA$. $Co(OAc)_2{\cdot}4H_2O$ (103 mg, 0.41 mmol) was added to a stirred deoxygenated solution of MeOH (10 mL) containing freshly deprotected DAB-$H_4{\cdot}4\,TFA$ and DFP (55.6 mg, 0.41 mmol). The reaction mixture was heated at 65 °C for 96 h, under an inert atmosphere, after which time it was allowed to cool to room temperature and the solvent was evaporated off under reduced pressure, followed by subsequent additions and removals of MeOH (3×5 mL), leaving the crude product as an orange solid. The crude product was purified by crystallization using vapor diffusion of degassed Et_2O into a solution of the crude $Co^{II}BR{\cdot}12\,TFA$ in degassed MeOH. Orange crystals were isolated by filtration and washing with Et_2O to afford pure $Co^{II}BR{\cdot}12\,TFA$ as an orange powder (117 mg, 36 %). UV/Vis (MeOH, 2.0×10^{-6} M): λ_{max} ($\log\varepsilon$) = 231 (5.44), 293 (4.90), 303 (4.87), 319 nm sh; UV/Vis (MeOH, 5.57×10^{-4} M): λ_{max} ($\log\varepsilon$) = 706 nm (2.18).; HRMS (ESI): *m*/*z* (%): 2234.5859 (5) $[M-2CF_3CO_2]^{2+}$, 1451.9632 (100) $[M-3CF_3CO_2]^{3+}$, 1060.9506 (35) $[M-4CF_3CO_2]^{4+}$.

$Mn^{II}BR{\cdot}12\,TFA$: Boc-DAB (310 mg, 0.519 mmol) was dissolved in trifluoroacetic acid (2 mL) and stirred at room temperature for 10 min. Excess trifluoroacetic acid was removed by rotary evaporation under reduced pressure, followed by subsequent additions and removals of MeOH (3×5 mL), leaving a pink tar containing DAB-$H_4{\cdot}4\,TFA$. $Mn(OAc)_2$ (127 mg, 0.519 mmol) was added to a stirred solution of *i*PrOH (5 mL) containing freshly deprotected DAB-$H_4{\cdot}4\,TFA$ and DFP (70 mg, 0.519 mmol) and the reaction mixture was heated at 70 °C for 72 h, producing a yellow-colored precipitate, which was removed by filtration, washed with *i*PrOH and Et_2O, and then dried to afford a yellow powder (281 mg, 70 %). The product was crystallized from a solution in MeOH (2 mL) into which Et_2O was allowed to diffuse slowly. UV/Vis (MeOH, 3.43×10^{-6} M): λ_{max} ($\log\varepsilon$) = 228 (5.63), 291 (4.99), 301 (4.99), 321 nm (4.56); UV/Vis (MeOH, 6.98×10^{-4} M): λ_{max} ($\log\varepsilon$) = 401 (2.94), 428 (2.93), 451 nm (2.94); HRMS (ESI): *m*/*z* (%): 1443.9618 (100) $[M-3CF_3CO_2]^{3+}$, 1054.6730 (70) $[M-4CF_3CO_2]^{4+}$, 821.1694 (40) $[M-5CF_3CO_2]^{5+}$.

$Cd^{II}BR{\cdot}12\,TFA$ and $Cd^{II}SK{\cdot}8\,TFA$: Boc-DAB (52.5 mg, 0.088 mmol) was dissolved in trifluoroacetic acid (2 mL) and stirred at room temperature for 10 min. Excess trifluoroacetic acid was removed by rotary evaporation under reduced pressure, followed by subsequent additions and removals of MeOH (3×5 mL), leaving a pink tar containing DAB-$H_4{\cdot}4\,TFA$. $Cd(OAc)_2$ (20.2 mg, 0.088 mmol) was added to a stirred solution of *i*PrOH (5 mL) containing freshly deprotected DAB-$H_4{\cdot}4\,TFA$ and DFP (11.8 mg, 0.088 mmol). The reaction mixture was heated at 65 °C for 12 h to produce an off-white-colored precipitate, which was removed by filtration, washed with *i*PrOH and Et_2O, and dried, affording a white powder. The white powder was shown, by direct integration of the signals in the ^1H NMR spectrum, to contain $Cd^{II}SK{\cdot}8\,TFA$ and $Cd^{II}BR{\cdot}12\,TFA$ in a 0.9:1 ratio. ^1H NMR (600 MHz, CD_3OD, 298 K): δ = 6.37 (br s, 2H), 6.46 (d, J = 12 Hz, 4H), 6.60 (d, J = 12 Hz, 4H), 6.75 (d, J = 6 Hz, 4H), 6.86 (d, J = 6 Hz, 4H) 7.23 (br s, 2H), 7.83 (br s, 2H), 8.08 (br s, 2H), 8.27 (d, J = 12 Hz, 2H), 8.30 (d, J = 12 Hz, 6H), 8.58 (t, J = 6 Hz, 1H), 8.59 (t, J = 6 Hz, 1H), 8.70 (s, 2H), 8.90 ppm (s, 2H); HRMS (ESI): *m*/*z* (%): 1588.1758 (52) $[M_{BR}-3CF_3CO_2]^{3+}$, $[M_{SK}-2CF_3CO_2]^{2+}$, 1141.1369 (24) $[M_{BR}-4CF_3CO_2]^{4+}$, 1001.7761 (100) $[M_{SK}-3CF_3CO_2]^{3+}$.

$Zn^{II}SK{\cdot}8TFA$: Boc-DAB (1.21 g, 2.03 mmol) was dissolved in neat trifluoroacetic acid (60 mL) and stirred at room temperature for 30 min. Excess trifluoroacetic acid was removed under reduced pressure, followed by subsequent additions and removals of MeOH (3×60 mL), leaving a pink tar containing DAB-$H_4{\cdot}4$TFA. $Zn(OAc)_2$ (0.372 g, 2.03 mmol) was added simultaneously with stirring to solution in *i*PrOH (60 mL) containing freshly deprotected DAB-$H_4{\cdot}4$TFA, followed by the addition of DFP (0.274 g, 2.03 mmol). The reaction mixture was heated at 60 °C for 32 h, producing a pale-yellow solution along with a light-purple precipitate. The mixture was allowed to cool to room temperature, and the precipitate was removed by filtration, washed with *i*PrOH (3×30 mL) and Et_2O (3×30 mL). This procedure afforded a mixture of $Zn^{II}BR{\cdot}12$TFA and $Zn^{II}SK{\cdot}8$TFA, in a 4:1 ratio as indicated by ^{1}H NMR spectroscopy, as a pale-purple powder (1.38 g). Crystals of $Zn^{II}SK{\cdot}8$TFA, suitable for X-ray crystallography, were grown by vapor diffusion of Et_2O into a solution of the powder in 3:1 *n*PrOH/MeOH and separated manually from crystals of $Zn^{II}BR{\cdot}12$TFA. ^{1}H NMR (600 MHz, CD_3OD, 298 K): δ = 4.77 (d, J = 14 Hz, 8H), 4.84 (d, J = 14 Hz, 8H), 6.60 (d, J = 8.3 Hz, 16H), 6.64 (d, J = 7.9 Hz, 16H), 7.33 (d, J = 2.4 Hz, 8H), 8.15 (br s, 8H), 8.25 (d, J = 1.9 Hz, 8H), 8.36 (d, J = 7.9 Hz, 8H), 8.67 (t, J = 7.8 Hz, 4H), 8.93 ppm (s, 8H); HRMS (ESI): m/z (%): 1464.582 (100) $[M-3CF_3CO_2]^{3+}$, 938.6121 (30) $[M-3CF_3CO_2]^{3+}$.

Acknowledgements

The research was supported by the US National Science Foundation (NSF) under grant number CHE-0924620.

[1] E. Wasserman, *J. Am. Chem. Soc.* **1960**, *82*, 4433–4434; E. Wasserman, *Bell Lab. Rec.* **1960**, 394.

[2] A [2]catenane is a compound containing molecules comprised of two mutually interlocked rings. When the molecules also serve as a ligand for a metal ion, the compound is referred to as a [2]catenate, and the ligand, a [2]catenand, see: C. O. Dietrich-Buchecker, J.-P. Sauvage, J.-M. Kern, *J. Am. Chem. Soc.* **1984**, *106*, 3043–3045. Note that the digit inside the square brackets refers to the number of interlocked rings in the molecule.

[3] a) H. L. Frisch, E. Wasserman, *J. Am. Chem. Soc.* **1961**, *83*, 3789–3795; b) S. J. Tauber, *J. Res. Natl. Bur. Stand. Sect. A* **1963**, *67 A*, 591–599; c) J. Simon, *Proc. Symp. Appl. Math.* **1992**, *45*, 97–130; d) N. van Gulick, *New J. Chem.* **1993**, *17*, 619–625; e) C. Liang, K. Mislow, *J. Math. Chem.* **1994**, *16*, 27–35; f) J. S. Siegel, *Science* **2004**, *304*, 1256–1258; g) E. E. Fenlon, *Eur. J. Org. Chem.* **2008**, 5023–5035; h) D. B. Amabilino, L. Pérez-García, *Chem. Soc. Rev.* **2009**, *38*, 1562–1571.

[4] a) V. I. Sokolov, *Russ. Chem. Rev.* **1973**, *42*, 452–463; b) D. M. Walba, *Tetrahedron* **1985**, *41*, 3161–3212; c) K. Mislow, *Top. Stereochem.* **1999**, *22*, 1–82.

[5] For an overview of interlocked molecules, see: a) D. B. Amabilino, J. F. Stoddart, *Chem. Rev.* **1995**, *95*, 2725–2828; b) *Molecular Catenanes, Rotaxanes and Knots* (Eds.: J.-P. Sauvage, C. Dietrich-Buchecker), Wiley-VCH, Weinheim, **1999**; c) F. M. Raymo, J. F. Stoddart, *Chem. Rev.* **1999**, *99*, 1643–1663; d) M. Fujita, *Acc. Chem. Res.* **1999**, *32*, 53–61; e) J. P. Collin, C. Dietrich-Buchecker, P. Gaviña, M. C. Jiminez-Molero, J.-P. Sauvage, *Acc. Chem. Res.* **2001**, *34*, 477–487; f) G. Kaiser, T. Jarrosson, S. Otto, Y.-F. Ng, A. D. Bond, J. K. M. Sanders, *Angew. Chem.* **2004**, *116*, 1993–1996; *Angew. Chem. Int. Ed.* **2004**, *43*, 1959–1962; g) L. Wang, M. O. Vysotsky, A. Bogdan, M. Bolte, V. Böhmer, *Science* **2004**, *304*, 1312–1314; h) C. A. Schalley, T. Weilandt, J. Brüggermann, F. Vögtle, *Top. Curr. Chem.* **2004**, *232–242*, 141–200; i) M. S. Vickers, P. D. Beer, *Chem. Soc. Rev.* **2007**, *36*, 211–225; j) M. A. Olson, Y. Y. Botros, J. F. Stoddart, *Pure Appl. Chem.* **2010**, *82*, 1569–1574.

[6] Note that the strength of a mechanical bond equates with the strength of the weakest covalent or coordinative bond in the molecule. See: a) J. F. Stoddart, H. M. Colquhoun, *Tetrahedron* **2008**, *64*, 8231–8263; b) J. F. Stoddart, *Chem. Soc. Rev.* **2009**, *38*, 1802–1820.

[7] a) D. H. Busch, N. A. Stephenson, *Coord. Chem. Rev.* **1990**, *100*, 119–154; b) S. Anderson, H. L. Anderson, J. K. M. Sanders, *Acc. Chem. Res.* **1993**, *26*, 469–475; c) R. Cacciapaglia, L. Mandolini, *Chem. Soc. Rev.* **1993**, *22*, 221–231; d) R. Hoss, F. Vögtle, *Angew. Chem.* **1994**, *106*, 389–398; *Angew. Chem. Int. Ed. Engl.* **1994**, *33*, 375–384; e) J. P. Schneider, J. W. Kelly, *Chem. Rev.* **1995**, *95*, 2169–2187; f) F. M. Raymo, J. F. Stoddart, *Pure Appl. Chem.* **1996**, *68*, 313–322; g) M. Fujita, *Chem. Soc. Rev.* **1998**, *27*, 417–425; h) G. A. Breault, C. A. Hunter, P. C. Mayers, *Tetrahedron* **1999**, *55*, 5265–5293; i) *Templated Organic Synthesis* (Eds.: F. Diederich, P. J. Stang), Wiley-VCH, Weinheim, **2000**; j) T. J. Hubin, D. H. Busch, *Coord. Chem. Rev.* **2000**, *200*, 5–52; k) J. F. Stoddart, H.-R. Tseng, *Proc. Natl. Acad. Sci. USA* **2002**, *99*, 4797–4800; l) M.-J. Blanco, J.-C. Chambron, M. C. Jiménez, J.-P. Sauvage, *Top. Stereochem.* **2002**, *23*, 125–173; m) D. H. Busch, *Top. Curr. Chem.* **2005**, *249*, 1–65; n) F. Arićo, J. D. Badjić, S. J. Cantrill, A. H. Flood, K. C.-F. Leung, Y. Liu, J. F. Stoddart, *Top. Curr. Chem.* **2005**, *249*, 203–259; o) S. J. Cantrill, R. H. Grubbs, D. Lanari, K. C.-F Leung, A. Nelson, K. G. Poulin-Kerstien, S. P. Smidt, J. F. Stoddart, D. A. Tirrell, *Org. Lett.* **2005**, *7*, 4213–4216; p) B. H. Northrop, F. Arićo, N. Tangchaivang, J. D. Badjić, J. F. Stoddart, *Org. Lett.* **2006**, *8*, 3899–3902; q) A. R. Williams, B. H. Northrop, T. Chang, J. F. Stoddart, A. J. P. White, D. J. Williams, *Angew. Chem.* **2006**, *118*, 6817–6821; *Angew. Chem. Int. Ed.* **2006**, *45*, 6665–6669; r) C. D. Meyer, C. S. Joiner, J. F. Stoddart, *Chem. Soc. Rev.* **2007**, *36*, 1705–1723; s) K. E. Griffiths, J. F. Stoddart, *Pure Appl. Chem.* **2008**, *80*, 485–506; t) J. D. Crowley, S. M. Goldup, A.-L. Lee, D. A. Leigh, R. T. McBurney, *Chem. Soc. Rev.* **2009**, *38*, 1530–1541.

[8] a) J.-M. Lehn, *Supramolecular Chemistry: Concepts and Perspectives*, VCH, Weinheim, **1995**, Chapter 2; b) *Comprehensive Supramolecular Chemistry, Vol. 1* (Eds.: J. L. Atwood, J. E. D. Davies, D. D. MacNicol, F. Vögtle), Pergamon, Oxford, **1996**; c) M. A. Garcia-Garibay, *Curr. Opin. Solid State Mater. Sci.* **1998**, *3*, 399–406; d) A. N. M. M. Rahman, R. Bishop, D. C. Craig, M. L. Scudder, *Eur. J. Org. Chem.* **2003**, 72–81; e) L. R. Nassimbeni, *Acc. Chem. Res.* **2003**, *36*, 631–637; f) A. Angeloni, P. C. Crawford, A. G. Orpen, T. J. Podesta, B. J. Shore, *Chem. Eur. J.* **2004**, *10*, 3783–3791; g) P. Metrangolo, H. Neukirch, T. Pilati, G. Resnati, *Acc. Chem. Res.* **2005**, *38*, 386–395; h) J. F. Stoddart, *Nat. Chem.* **2009**, *1*, 14–15.

[9] a) B. Hasenknopf, J.-M. Lehn, N. Boumediene, A. Dupont-Gervais, A. Van Dorsselaer, B. Kneisel, D. Fenske, *J. Am. Chem. Soc.* **1997**, *119*, 10956–10962; b) D. M. Bassani, J.-M. Lehn, S. Serroni, F. Puntoriero, S. Campagna, *Chem. Eur. J.* **2003**, *9*, 5936–5946; c) R. W. Saalfrank, C. Deutscher, H. Maid, A. M. Ako, S. Sperner, T. Nakajima, W. Bauer, F. Hampel, B. A. Heß, N. J. R. van Eikema Hommes, R. Puchta, F. W. Heinmann, *Chem. Eur. J.* **2004**, *10*, 1899–1905; d) J. R. Nitschke, *Acc. Chem. Res.* **2007**, *40*, 103–112.

[10] a) S. J. Rowan, S. J. Cantrill, G. R. L. Cousins, J. K. M. Sanders, J. F. Stoddart, *Angew. Chem.* **2002**, *114*, 938–993; *Angew. Chem. Int. Ed.* **2002**, *41*, 898–952; b) R. L. E. Furlan, S. Otto, J. K. M. Sanders, *Proc. Natl. Acad. Sci. USA* **2002**, *99*, 4801–4804; c) P. T. Corbett, J. Leclaire, L. Vial, K. R. West, J.-L. Wietor, J. K. M. Sanders, S. Otto, *Chem. Rev.* **2006**, *106*, 3652–3711; d) J.-M. Lehn, *Chem. Soc. Rev.* **2007**, *36*, 151–160; e) P. C. Haussmann, J. F. Stoddart, *Chem. Rec.* **2009**, *9*, 136–154.

[11] a) V. Balzani, A. Credi, F. Raymo, J. F. Stoddart, *Angew. Chem.* **2000**, *112*, 3484–3530; *Angew. Chem. Int. Ed.* **2000**, *39*, 3348–3391; b) A. R. Pease, J. O. Jeppesen, J. F. Stoddart, Y. Luo, C. P. Collier, J. R. Heath, *Acc. Chem. Res.* **2001**, *34*, 433–444; c) E. R. Kay, D. A. Leigh, F. Zerbetto, *Angew. Chem.* **2007**, *119*, 72–196; *Angew. Chem. Int. Ed.* **2007**, *46*, 72–191; d) B. Champin, P. Mobian, J.-P. Sauvage, *Chem. Soc. Rev.* **2007**, *36*, 358–366; e) V. Balzani, M. Venturi, A. Credi, *Molecular Devices and Machines: Concepts and Perspectives for the Nanoworld*, Wiley, New York, **2008**; f) R. Klajn, J. F. Stoddart, B. A. Grzybowski, *Chem. Soc. Rev.* **2010**, *39*, 2203–2237.

[12] a) D. B. Amabilino, P. R. Ashton, A. S. Reder, N. Spencer, J. F. Stoddart, *Angew. Chem.* **1994**, *106*, 1316–1319; *Angew. Chem. Int. Ed.*

Engl. **1994**, *33*, 1286–1290; b) D. B. Amabilino, P. R. Ashton, V. Balzani, S. E. Boyd, A. Credi, J. Y. Lee, S. Menzer, J. F Stoddart, M. Venturi, D. J. Williams, *J. Am. Chem. Soc.* **1998**, *120*, 4295–4307.

[13] D. B. Amabilino, P. R. Ashton, S. E. Boyd, J. Y. Lee, S. Menzer, J. F. Stoddart, D. J. Williams, *Angew. Chem.* **1997**, *109*, 2160–2162; *Angew. Chem. Int. Ed. Engl.* **1997**, *36*, 2070–2072.

[14] L. R. Rose, *Seeing Solomon's Knot*, Lois Rose, Los Angeles, **2005**.

[15] a) D. Rolfsen, *Knots and Links*, Publish or Perish, Berkeley, **1976**; b) C. C. Adams, *The Knot Book*, Freeman, New York, **1994**; c) D. Andrae, *New J. Chem.* **2006**, *30*, 873–882.

[16] a) J.-F. Nierengarten, C. O. Dietrich-Buchecker, J.-P. Sauvage, *J. Am. Chem. Soc.* **1994**, *116*, 375–376; b) F. Ibukuro, M. Fujita, K. Yamaguchi, J.-P. Sauvage, *J. Am. Chem. Soc.* **1999**, *121*, 11014–11015; c) C. P. McArdle, J. J. Vittal, R. J. Puddephatt, *Angew. Chem.* **2000**, *112*, 3977–3980; *Angew. Chem. Int. Ed.* **2000**, *39*, 3819–3822; d) C. Peinador, V. Blanco, J. M. Quintela, *J. Am. Chem. Soc.* **2009**, *131*, 920–921; e) T. K. Ronson, J. Fisher, L. P. Harding, P. J. Rizkallah, J. E. Warren, M. J. Hardie, *Nat. Chem.* **2009**, *1*, 212–216.

[17] SKs, which are 4_1^2 links, can be thought of as [2]catenanes, which are 2_1^2 links, wherein the two rings crossover at four nodes rather than two, to give the doubly interlocked structure.

[18] P. Cromwell, E. Beltrami, M. Rampichini, *Math. Intelligencer* **1998**, *20*, 53–62; other examples are highlighted in greater detail on the world wide web, see: http://www.Liv.ac.uk/~spmr02/rings/index.html.

[19] a) C. A. Schalley, *Angew. Chem.* **2004**, *116*, 4499–4501; *Angew. Chem. Int. Ed.* **2004**, *43*, 4399–4401; b) S. J. Cantrill, K. S. Chichak, A. J. Peters, J. F. Stoddart, *Acc. Chem. Res.* **2005**, *38*, 1–9.

[20] C. Liang, K. Mislow, *J. Math. Chem.* **1995**, *18*, 1–24.

[21] a) A. Ruzmaikin, P. Akhmetiev, *Phys. Plasmas* **1994**, *1*, 331–336; b) S. M. Austin, G. F. Bertsch, *Sci. Am.* **1995**, *272*, 90–95; c) B. V. Danilin, T. Rogde, J. S. Vaagen, I. J. Thompson, M. V. Zhukov, *Phys. Rev. C* **2004**, *69*, 024609/1–10.

[22] a) C. Mao, W. Sun, N. C. Seeman, *Nature* **1997**, *386*, 137–138; b) N. C. Seeman, *Angew. Chem.* **1998**, *110*, 3408–3428; *Angew. Chem. Int. Ed.* **1998**, *37*, 3220–3238.

[23] For an examination of previously unnoticed BR topologies in framework materials, see: a) L. Carlucci, G. Ciani, D. M. Proserpio, *CrystEngComm* **2003**, *5*, 269–279; for further examples, see: b) L. Dobrzańska, H. G. Raubenheimer, L. J. Barbour, *Chem. Commun.* **2005**, 5050–5052; c) R. Liantonio, P. Metrangolo, F. Meyer, T. Pilati, W. Navarrini, G. Resnati, *Chem. Commun.* **2006**, 1819–1821; d) X.-Q. Lu, M. Pan, J.-R. He, Y.-P. Cai B.-S. Kang, C.-Y. Su, *CrystEngComm* **2006**, *8*, 847–849; e) J. Li, L. Song, S. Du, *Inorg. Chem. Commun.* **2007**, *10*, 358–361; f) X.-L. Zhang, C.-P. Guo, Q.-Y. Yang, W. Wang, W.-S. Liu, B.-S. Kang, C.-Y. Su, *Chem. Commun.* **2007**, 4242–4244; g) X.-L. Zhang, C.-P. Guo, Q.-Y. Yang, T.-B. Lu, Y.-X. Tong, C.-Y. Su, *Chem. Mater.* **2007**, *19*, 4630–4632; h) Q.-Y. Yang, S.-R. Zheng, R. Yang, M. Pan, R. Cao, C.-Y. Su, *CrystEngComm* **2009**, *11*, 680–685; i) P. Byrne, G. O. Lloyd, N. Clarke, J. W. Steed, *Angew. Chem.* **2008**, *120*, 5845–5848; *Angew. Chem. Int. Ed.* **2008**, *47*, 5761–5764; j) J.-J. Jang, L. Li, T. Yang, D.-B. Kuang, W. Wang, C.-Y. Su, *Chem. Commun.* **2009**, 2387–2389; k) Y.-B. Men, J. Sun, Z.-T. Huang, Q.-Y. Zheng, *Angew. Chem.* **2009**, *121*, 2917–2920; *Angew. Chem. Int. Ed.* **2009**, *48*, 2873–2876; l) Q.-X. Yao, X.-H. Jin, Z.-F. Ju, H.-X. Zhang, J. Zhang, *CrystEngComm* **2009**, *11*, 1502–1504; m) N. N. Adarsh, P. Dastidar, *Cryst. Growth Des.* **2010**, *10*, 483–487.

[24] a) S.-H. Chiu, A. R. Pease, J. F. Stoddart, A. J. P. White, D. J. Williams, *Angew. Chem.* **2002**, *114*, 280–284; *Angew. Chem. Int. Ed.* **2002**, *41*, 270–274; b) M. Schmittel, A. Ganz, D. Fenske, *Org. Lett.* **2002**, *4*, 2289–2292; c) J. C. Loren, M. Yoshizawa, R. F. Haldimann, A. Linden, J. S. Siegel, *Angew. Chem.* **2003**, *115*, 5880–5883; *Angew. Chem. Int. Ed.* **2003**, *42*, 5702–5705; d) Y. Liu, *Tetrahedron Lett.* **2007**, *48*, 3871–3874; e) R. S. Forgan, J. M. Spruell, J.-C. Olsen, C. L. Stern, J. F. Stoddart, *J. Mex. Chem. Soc.* **2009**, *53*, 134–138; f) R. S. Forgan, D. C. Friedman, C. L. Stern, C. J. Bruns, J. F. Stoddart, *Chem. Commun.* **2010**, *46*, 5861–5863.

[25] We use the term "ring-in-ring" complex to describe only assemblies in which the macrocycles are arranged in an approximately perpendicular fashion. These compounds are considerably rarer than the more familiar "macrocycle-within-macrocycle" architectures.

[26] T. J. Hubin, A. G. Kolchinski, A. L. Vance, D. H. Busch, *Adv. Supramol. Chem.* **1999**, *6*, 237–357.

[27] K. S. Chichak, S. J. Cantrill, A. R. Pease, S.-H. Chiu, G. W. V. Cave, J. L. Atwood, J. F. Stoddart, *Science* **2004**, *304*, 1308–1312.

[28] K. S. Chichak, A. J. Peters, S. J. Cantrill, J. F. Stoddart, *J. Org. Chem.* **2005**, *70*, 7956–7962.

[29] C. D. Pentecost, K. S. Chichak, A. J. Peters, G. W. V. Cave, S. J. Cantrill, J. F. Stoddart, *Angew. Chem.* **2007**, *119*, 222–226; *Angew. Chem. Int. Ed.* **2007**, *46*, 218–222.

[30] We have proposed that BR compounds that are assembled using metal ions, and that retain these metal ions as an intrinsic part of their structure, be referred to as Borromeates.[31]

[31] A. J. Peters, K. S. Chichak, S. J. Cantrill, J. F. Stoddart, *Chem. Commun.* **2005**, 3394–3396.

[32] Whereas it was possible to prepare crystalline samples of Mn^{II}BR·12TFA, their weakly diffracting nature precluded structural characterization by single-crystal X-ray diffraction analysis.

[33] Data were collected on a Bruker SMART 1000 CCD diffractometer with $Mo_{K\alpha}$ radiation using the ω-scan mode. Data were corrected for absorption by using the SADABS program and structure solution and refinement were performed by using the SHELX-97 software package. All non-hydrogen atoms except the solvent molecules were refined anisotropically while the hydrogen atoms were included at geometrically calculated positions and allowed to ride on their parent atoms. CCDC-277849 (Cu^{II}BR·12TFA) and 277848 (Co^{II}BR·12TFA) contain the supplementary crystallographic data for this paper. These data can be obtained free of charge from The Cambridge Crystallographic Data Centre via www.ccdc.cam.ac.uk/data_request/cif.

[34] Single crystals suitable for X-ray crystallographic analysis were grown by vapor diffusion of Et_2O into a solution of Cu^{II}BR·12TFA in MeOH. A green single crystal was attached with oil to a thin glass fiber. Suitable crystals were extremely difficult to mount; solvent loss was immediately evident as soon as the crystal was removed from the mother liquor. Crystal data for $[(C_{62}H_{46}N_{10}O_4)_3\cdot(CuO_2CCF_3)_6]\cdot 6(CF_3CO_2)\cdot 6(CH_3OH)\cdot 6(H_2O)$: trigonal, $a=b=34.0854(9)$ Å, $c=22.0678(12)$ Å, $V=22203.7(15)$ Å^3, space group $R\bar{3}$, $Z=3$, $\rho_{calcd}=1.124$ g cm^{-3}, $\lambda(Mo_{K\alpha})=0.70930$ Å, $F(000)=7650$, $T=173(2)$ K, 10085 unique reflections ($2\theta\leq 56°$), of which 4643 were observed [$I_o>2\sigma(I)$]. Final R factors: $R_1=0.1802$, $wR_2=0.4472$ for 403 parameters.

[35] Single crystals suitable for X-ray crystallographic analysis were grown by vapor diffusion of Et_2O into a solution of Co^{II}BR·12TFA in MeOH. A yellow single crystal was attached with oil to a thin glass fiber. Suitable crystals were extremely difficult to mount; solvent loss was immediately evident as soon as the crystal was removed from the mother liquor. Crystal data for $[(C_{62}H_{46}N_{10}O_4)_3\cdot(CoO_2CCF_3)_6]\cdot 6(CF_3CO_2)\cdot 13(CH_3OH)\cdot 3(H_2O)$: triclinic, $a=19.458(9)$ Å, $b=20.323(9)$ Å, $c=22.623(10)$ Å, $\alpha=107.829(7)°$, $\beta=115.106(7)°$, $\gamma=96.807(7)°$, $V=7385(6)$ Å^3, space group $P\bar{1}$, $Z=1$, $\rho_{calcd}=1.059$ g cm^{-3}, $\lambda(Mo_{K\alpha})=0.70930$ Å, $F(000)=2420$, $T=173(2)$ K, 31765 unique reflections ($2\theta\leq 56°$), of which 6868 were observed [$I_o>2\sigma(I)$]. Final R factors: $R_1=0.1217$, $wR_2=0.3285$ for 1506 parameters. Owing to the low parameter/observation ratio 75 restraints had to be imposed on the molecule.

[36] It has not gone unnoticed that the packing efficiency of the six MeOH molecules within the $Co^{II}BR^{12+}$ cavity, 85%, far exceeds the ideal value of 55% proposed by Rebek et al. The 55% solution was formulated for dynamic host–guest complexes in solution, rather than solid-state assemblies, which may explain the difference in packing coefficients. See: S. Mecozzi, J. Rebek, Jr., *Chem. Eur. J.* **1998**, *4*, 1016–1022. All cavity and packing volumes were determined computationally by using the software packages MCAVITY and X-Seed, see: L. J. Barbour, MCAVITY—Molecular Cavity Calculator, **2003** and L. J. Barbour, *J. Supramol. Chem.* **2001**, *1*, 189–191.

[37] a) P. Manikandan, K. R. J. Thomas, P. T. Manoharan, *J. Chem. Soc. Dalton Trans.* **2000**, 2779–2785; b) J. M. Holland, X. Liu, J. P. Zhao, F. E. Mabbs, C. A. Kilner, M. Thornton-Pett, M. A. Halcrow, *J. Chem. Soc. Dalton Trans.* **2000**, 3316–3324; c) D. S. Marlin, M. M. Olmstead, P. K. Mascharak, *Inorg. Chem.* **2001**, *40*, 7003–7008.

[38] Other solvents have led to the successful formation of BRs, including MeOH and EtOH (ref. [27]), yet not as efficiently as *i*PrOH. This solvent effect on the yield and purity is likely to result from the solubility differences of the product in these solvents. BRs are soluble in EtOH and MeOH, but are not soluble in *i*PrOH, and therefore, precipitate upon formation, kinetically trapping the BR product.

[39] We have modified the synthesis of molecular BRs to embrace undergraduate laboratory practical classes and have used the establishment of this teaching tool to have undergraduate students prepare molecular BRs on a gram scale. See: C. D. Pentecost, N. Tangchaivang, S. J. Cantrill, K. S. Chichak, A. J. Peters, J. F. Stoddart, *J. Chem. Educ.* **2007**, *84*, 855–859.

[40] The kinetically controlled self-assembly of two different donor–acceptor pseudorotaxanes on crystallization has been reported. See: B. H. Northrop, S. J. Khan, J. F. Stoddart, *Org. Lett.* **2006**, *8*, 2159–2162.

[41] A dramatic example of a kinetically controlled self-assembly process has been witnessed when, on crystallization from the appropriate solvent mixture, tetrabenzo[24]crown-8 and dibenzylammonium hexafluorophosphate form an array of [2]pseudorotaxanes stabilized by [C–H···F] hydrogen bonds to highly ordered, interstitially located PF_6^- anions. When the crystals of the [2]pseudorotaxane were dissolved in CD_3COCD_3, the 1:1 complex disassembled spontaneously at 25 °C with a half-life of 15.5 days, that is, $\Delta G^{\neq} = 26\ \mathrm{kcal\,mol^{-1}}$, see: a) P. R. Ashton, S. J. Cantrill, J. A. Preece, J. F. Stoddart, Z.-H. Wang, A. J. P. White, D. J. Williams, *Org. Lett.* **1999**, *1*, 1917–1920; b) S. J. Cantrill, J. A. Preece, J. F. Stoddart, Z.-H. Wang, A. J. P. White, D. J. Williams, *Tetrahedron* **2000**, *56*, 6675–6681.

[42] Colorless crystals were obtained from a mixture of long needles and block prism-shaped cubes. Suitable crystals were difficult to mount as the solvent loss was very rapid even when covered with viscous oils. A suitable block prism ($0.4\times0.4\times0.2$ mm) was picked on a nylon loop with oil and used for data collection at low temperature on a Bruker Smart 1000 diffractometer with an Apex11 detector. Data were collected with a 90 s exposure time per frame. Absorption corrections were performed with SADABS and SHELXTL software package was used for structure solution and refinement. Final difference maps showed some residual peaks of missing and or disordered solvents and were not accounted for in the treatment of the X-ray crystal data. On account of the extensive disorder of the trifluoroacetate anions and solvent molecules, the weighted *R* factor is high. CCDC-781947 contains the supplementary crystallographic data for this paper. These data can be obtained free of charge from The Cambridge Crystallographic Data Centre via www.ccdc.cam.ac.uk/data_request/cif. Crystal data for $[Zn_4(C_{124}H_{92}N_{20}O_8)(O_2CCF_3)_4\cdot4(O_2CCF_3)\cdot3(C_3H_8O)]$: orthorhombic, $a=23.294(3)$ Å, $b=28.744(3)$ Å, $c=53.008(7)$ Å, $V=35493(7)$ Å^3, space group *Fddd*, $Z=8$, $\rho_{calcd}=1.254\ \mathrm{g\,cm^{-3}}$, $\lambda(Mo_{K\alpha})=0.71073$ Å, $T=100(2)$ K, $F(000)=13592$, 12827 unique reflections ($2\theta_{max}=60.12°$) of which 7878 were observed [$I_o>2\sigma(I)$]. Final *R* factors: $R_1=0.0994$, $wR_2=0.3067$ for 487 parameters.

[43] J. Jacques, A. Collet, S. H. Wilen, *Enantiomers, Racemates and Resolutions*, Wiley-VCH, Weinheim, **1981**.

[44] At the time we first observed this additional species in the gas phase (see ref. [27]), we were not attuned to the possibility of a SK side product. Accordingly, when we occasionally observed the existence of another symmetrical, albeit minor product in the crude ^{1}H NMR spectrum, we suspected that these extra peaks corresponded to $Zn@Zn^{II}BR\cdot12TFA$. Now that we have studied this self-assembly process in considerable detail for five years, we can explain the situation in more detail with more authority. First of all, since we are certain now that these downfield peaks arise from the structure of $Zn^{II}SK\cdot8TFA$—and have repeated this experiment many more times—we note that SKs appear as a side product far more often than $Zn@Zn^{II}BR\cdot12TFA$. Second, we have obtained X-ray crystallographic data of functionalized BRs with zinc ions occupying the interstitial sites of the crystalline superstructure. See: C. R. Yates, D. Benítez, S. I. Khan, J. F. Stoddart, *Org. Lett.* **2007**, *9*, 2433–2436. Thus, it is possible that instead of, or in addition to, a species existing as a "filled" BR, in which the zinc ion resides within the cavity, the cation could also be located in the periphery of the BRs. Until we are successful or otherwise in isolating the $Zn@Zn^{II}BR\cdot12TFA$ as a discrete entity, we must remain guarded as to how this species would manifest itself in a ^{1}H NMR spectrum: we continue to suspect that it exists, at least in the gas phase!

[45] The highest symmetry the SK can possess is that belonging to the D_4 point group. Inspection of the solid-state X-ray crystal structure of $Zn^{II}SK\cdot8TFA$ reveals a D_2 symmetric conformation, and we are curious as to the conformation it occupies in solution. This question becomes more pertinent upon revisiting the ^{1}H NMR spectrum recorded at in CD_3OD at 300 K, which contains 10 signals, in agreement with either 1) the SK adopting the higher symmetry D_4 conformation in solution or 2) D_4 symmetry being the averaged situation in solution. For example, in the D_4 symmetric SK, all imine protons are equivalent, whereas, in the D_2 symmetric SK, two unique imine protons should be observed. The $Zn^{II}SK^{8+}$ backbone can interconvert between these two conformations through the same "chair flip" mechanism we have observed in the BRs, where the apex of each macrocycle changes its relative orientation about the methylene carbon next to the imine function. In ^{1}H NMR spectra (see the Supporting Information) collected as the sample was cooled to 233 K, we observed that all of the signals were significantly broadened, and, when collected at 213 K, the spectra showed the separation of some resonances into new signals. We therefore suggest that at room temperature $Zn^{II}SK\cdot8TFA$ changes conformations faster than can be observed on the 600 MHz NMR timescale, and thus we observe an overall averaged symmetry of D_4. However, in the process of cooling the sample to 213 K, perhaps some of the D_2 symmetric conformations freeze out, giving rise to a larger number of signals.

[46] As part of our efforts to characterize $Cu^{II}/Zn^{II}SK\cdot8TFA$ more fully, we did acquire a ^{1}H NMR spectrum of $Cu^{II}/Zn^{II}SK\cdot8TFA$, and reported it in the Supporting Information of reference [29]. Because Cu^{II} is paramagnetic, the signals were too broad to assign the with any amount of precision. For this reason, we also characterized $Cu^{II}/Zn^{II}SK\cdot8TFA$ by using electron paramagnetic resonance (EPR) spectroscopy, and observed a $g_{II}>g_{\perp}$ tensor pattern characteristic of similar tetragonally elongated copper complexes.

Received: June 25, 2010
Published online: October 22, 2010

